Competing magnetic instabilities in the weak itinerant antiferromagnetic TiAu

Wen Fong Goh and Warren E. Pickett
Department of Physics, University of California, Davis, California 95616, USA
(Received 12 May 2016; revised manuscript received 20 April 2017; published 16 May 2017; corrected 28 July 2017)

The binary intermetallic compound TiAu is distinguished by an extremely sharp and narrow density of states peak at the Fermi level that has been proposed, via scattering between mirrored van Hove singularities, to be the mechanism for antiferromagnetic ordering versus the more fundamental ferromagnetic Stoner instability. Here we study, using density functional theory methods, magnetic tendencies and effects of doping, the latter within the virtual crystal approximation (VCA). Ferromagnetic tendencies are quantified using the fixed spin moment approach, illustrating the strong Stoner instability that does not, however, provide the ground state. Use of VCA results allows the identification of the value of the Stoner exchange constant $\mathcal{I} = 0.74$ eV for Ti. Magnetic fluctuations not included with semilocal density functionals are quantified with the procedure provided by Ortenzi and coauthors, with alloy concentrations corresponding to the quantum critical points reduced by a factor of three to five. Our results provide useful guidelines for experimental doping studies of TiAu.

DOI: 10.1103/PhysRevB.95.205124

I. INTRODUCTION

Among the variety of magnetic behaviors that have been reported for itinerant metals, weak ferromagnetism (wFM) is rare. Only a handful of itinerant magnetic compounds have been reported in conventional compounds, viz. $ZrZn_2$ [1], $TiBe_2$ [2,3], and off-stoichiometric Sr_3In, all comprised of nonmagnetic elements. Weak magnetism also occurs in heavy fermion and metallo-organic systems, where correlation effects are stronger and the mechanism may differ. The above-mentioned small group of wFMs also share another common origin: They arise from accidental van Hove singularities (vHs) that make the nonmagnetic state unstable to Stoner ferromagnetism [4], even though there is not enough spectral density to support a substantial ordered moment. The small moment both reflects and encourages strong magnetic fluctuations which conspire to keep the magnetic entropy small at the transition.

The occurrence of small ordered moment, often delicate, magnetism is beginning to become known as *fragile magnetism*. The term was applied early on in this manner by Gayathri *et al.* to some behavior in the doped-manganite $La_{0.7}Ca_{0.3}Mn_{1x}Co_xO_3$ system [5]. Fragile magnetism was also how the heavy fermion system of doped $CeRu_2Ge_2$ was characterized by Raymond and coworkers [6]. In more recent times, fragile magnetism was reintroduced as a description by Ueland *et al.* [7] of heavy fermion YbBiPt. This characterization is becoming more common, with nearly all cases being tuned by doping, pressure or strain, or magnetic field, and an overview has been provided by Canfield and Bud'ko [8].

A magnetic phenomenon even rarer than wFM is weak antiferromagnetism (wAFM), which involves the same issues plus ordering at a nonzero wave vector $\vec{Q}_{AFM}$. TiAu is a recently revisited system for which Svanidze *et al.* discovered that the orthorhombic form orders antiferromagnetically [9] below the Neel temperature, $T_N = 36$ K. TiAu displays a Curie-Weiss (CW) moment of $0.8\mu_B$. This size is about half that of a spin-half local moment ($1.73\mu_B$), though there is no reason for Ti to have a spin-half moment in TiAu since (as we show within) its $3d$ band is roughly 1/3 filled. It was one success of Moriya's self-consistent renormalized theory of itinerant spin fluctuations that it predicts a Curie-Weiss-like susceptibility over a wide temperature range [10,11]. Neutron diffraction reveals an ordered local moment of only $0.15\,\mu_B$/Ti, identifying TiAu as a weak moment system. Ordering is at a commensurate wave vector $\vec{Q}_{AFM} = (0, \frac{\pi}{b}, 0)$, i.e., a simple doubling of the cell along the $\vec{b}$ axis; see Fig. 1.

These properties identify TiAu as an itinerant but commensurate wAFM, whereas small itinerant moments are more often associated with incommensurate spin-density wave states. These observations open several questions: Is the small ordered moment indicative of remnant fluctuations well below T_N? Is the itinerant wAFM phase the result of Fermi surface nesting, and if so, why is it commensurate? Is the CW moment actually a Ti local moment as is needed for the standard spin fluctuation (Curie-Weiss) picture, or does it arise from interaction of longer range magnetic fluctuations as suggested initially by Moriya and collaborators and elaborated on occasionally since, such as for multiorbital models by Konno [12]? The small moment places the system near a quantum critical point (QCP). As for all weak magnets, it is anticipated that the magnetic ground state is strongly affected by spin fluctuations.

The theory of the unusual properties of a wAFM near the QCP has a substantial history, reviewed by Löhneysen *et al.* [13]. Moriya's self-consistent renormalization (SCR) theory of spin fluctuations [14] provides a useful guide for our purposes, as it ties the small $|\vec{q}|$ (for wave vectors $\vec{Q} + \vec{q}$ near the ordering wave vector $\vec{Q}$), small ω behavior to averages of various band structure and Fermi surface (FS) quantities, thus bringing the focus to the geometry, topology, and velocity field of the FS. Near the Neèl point, the interaction of temporal and spatial fluctuations around the nonmagnetic state are treated in a self-consistent random phase approximation manner, renormalizing the FS averages that characterize the fluctuations.

TiAu presents one distinctive feature in its nonmagnetic electronic structure: an extremely sharp peak in the density of states $N(E)$ at the Fermi level [9,15], arising from two closely spaced van Hove singularities [15]. Taken together with the exchange interaction, this large value of $N(E_F)$ at the Fermi level E_F ensures a (Stoner) magnetic instability,

usually manifest as a FM or wFM phase. The wAFM ground state requires a mechanism for selecting the AFM wave vector as well as avoiding the FM state. Such wave vectors in metals are almost invariably linked to the topology of the FS, in terms of a nesting wave vector that corresponds to a spin density wave (SDW) wave vector. Svanidze *et al.* suggested that the FS favors ordering at $\frac{2}{3}\vec{Q}_{AFM}$ versus the observed ordering at $\vec{Q}_{AFM}$.

In previous work [15], it was pointed out that mirrored van Hove singularities separated by $\vec{Q}$ lead to a small $|\vec{q}|$, small ω behavior of the antiferromagnetic susceptibility $\chi(\vec{Q}+\vec{q},\omega)$ that is identical in form to that of the ferromagnetic $\vec{Q}=0$ case. Without mirroring, e.g., with vHs rotated with respect to each other, the AFM susceptibility near criticality has the form obtained by Moriya (see the appendix). The Fermi surface nesting function $\xi(\mathbf{q})$, which measures the phase space for scattering through wave vector $\mathbf{q}$ from the FS to a copy of the FS displaced by $\mathbf{q}$, is given by ($E_F = 0$)

$$\xi_{\mathbf{q}} = \sum_k \delta(\varepsilon_{\mathbf{k}})\delta(\varepsilon_{\mathbf{k}+\mathbf{q}}) = \frac{\Omega}{(2\pi)^3}\int_{\mathscr{L}} \frac{d\mathscr{L}_{\mathbf{k}}}{|\vec{v}_{\mathbf{k}} \times \vec{v}_{\mathbf{k}+\mathbf{q}}|}. \quad (1)$$

The second form enables the interpretation as the integral over the line of intersection of the undisplaced FS and another FS displaced by $\mathbf{q}$, weighted by the reciprocal of the cross product of the two velocities. Large contributions arise from (i) regions of phase space with aligned or antialigned velocities, the classic FS nesting, or (ii) regions where one or (even better) both velocities are small, as at vHs. This latter case becomes relevant at the vHs of TiAu, where the large masses result in larger regions of small velocities than if the masses were small. Evaluation of this function for TiAu led to maxima only around the vHs spanning wave vectors, not at any Fermi surface nesting vectors [15]. The critical fluctuations arise from scattering between small vHs regions of the FS rather than large regions of FS nesting.

In this paper, we present first principles studies, with methods described in Sec. II, of the electronic structure and magnetic tendencies of TiAu, with the goal of illuminating behavior associated with its weak itinerant antiferromagnetism. Svanidze *et al.* [9] provided several characteristics of the electronic structure and magnetic energies of TiAu. In Sec. III, the electronic structure and especially the van Hove singularities near the Fermi level are studied, along with the tendencies for FM versus AFM ordering in the stoichiometric compound. These results, and previous work, are expanded on by considering in Sec. IV electron and hole doping with a virtual crystal approximation, and also fixed spin moment study to quantify the ferromagnetic instability. A method of accounting for spin fluctuations is applied in Sec. V, and discussion and a summary in Sec. VI complete the paper.

II. CRYSTALLOGRAPHIC STRUCTURE; THEORETICAL METHODS

Orthorhombic TiAu crystallizes in space group *Pmma* (51), pictured in Fig. 1. At 5 K, neutron diffraction provides lattice parameters [9] $a = 4.622$ Å, $b = 2.915$ Å and $c = 4.897$ Å. The atom positions are given in the caption to Fig. 1. The shortest distance between two Ti atoms is 2.91 along the $\vec{b}$ axis. However, the distance between Ti atoms in the $\vec{a}$-$\vec{c}$ plane is less that 2% larger, at 2.96 Å, so a Ti-chain picture is not appropriate. For the hexagonal close-packed structure of elemental Ti, the nearest neighbor distance is similar, 2.95 Å, indicating that direct $3d$ Ti-Ti exchange coupling from orbital overlap between near neighbors is expected in addition to the conventional RKKY (Ruderman-Kittel-Kasuya-Yoshida) coupling of Ti moments to more distant neighbors through the itinerant electronic system.

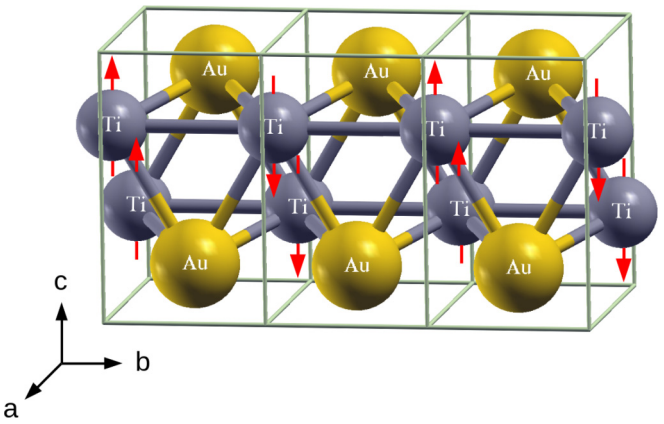

FIG. 1. Structure of *Pmma* TiAu with two f.u. per primitive cell; three primitive cells are shown. Antiferromagnet ordering with modulation vector $\vec{Q} = (0, \frac{\pi}{b}, 0)$ is shown. The positions of Ti and Au are at $2e$ (0.25, 0, 0.3110) and $2f$ (0.25, 0.5, 0.8176) sites, respectively.

Using the full-potential local-orbital minimum-basis code (FPLO [16]), we have carried out density functional theory (DFT) calculations on nonmagnetic TiAu and to situations that illuminate magnetism-related behavior. Due to the fine electronic structure, we have compared results obtained using the local density approximation (LDA) of Perdew and Wang [17] to those obtained from the generalized gradient approximation (GGA) of Perdew *et al.* [18] both in the scalar relativistic limit. Au $5d$,$6s$,$6p$ states and Ti $3d$,$4s$,$4p$ states were treated as the valence states, orthogonalized to the tightly bound core states. Density convergence to an accuracy of 10^{-6} was the conservative choice for the convergence condition, since in most cases the energy converges faster than the density. Most of the self-consistency calculations in this work were performed on a $20 \times 20 \times 20$ k-mesh. The density of states in Fig. 2 was obtained from a $60 \times 60 \times 60$ k-mesh, corresponding to 29 791 points in the irreducible wedge.

In weak magnets but also in select other cases, such as the ferro-pnictides and ferro-chalcogenides that become high-temperature superconductors when doped, it has been found that the commonly used semilocal exchange-correlation functionals overestimate the ordered moment. Moreover, one of the differences between GGA and LDA is that GGA enhances the exchange and usually gives larger moments than does LDA. Since the overestimate of exchange effects is less for LDA than for GGA, we present mostly results based on LDA, commenting in places on what would be obtained with GGA. As already reported [9] and as will be discussed here,

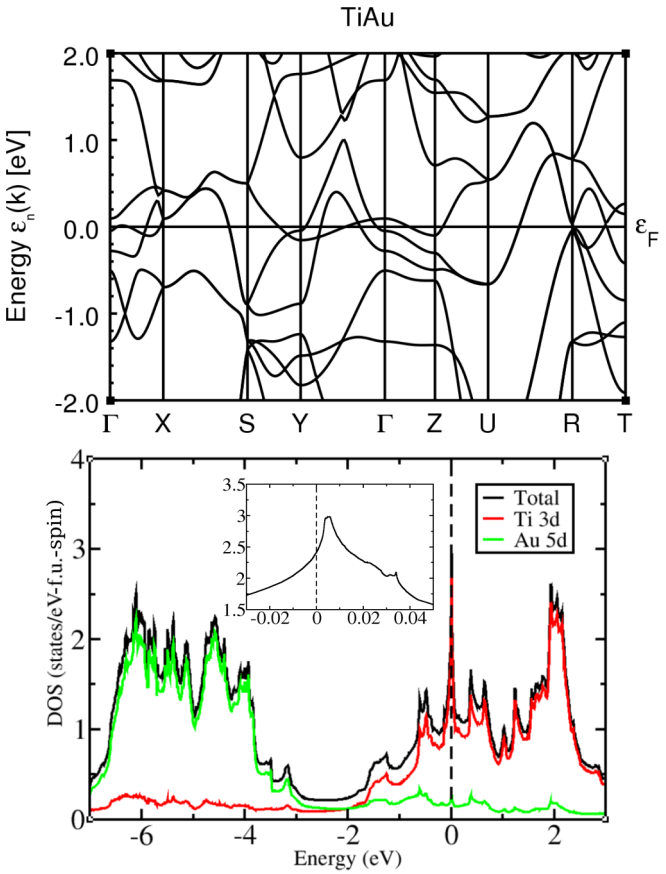

FIG. 2. Upper panel: The nonmagnetic band structure shows low dispersion along Γ-Z. The vHs does not lie on a high symmetry line. Lower panel: The total and atom-projected density of states (DOS), showing that the states from −7 to −2 eV arise from Au 5d orbitals, whereas the bands from −2 to 3 eV have Ti 3d character. Insert: The narrow and high peak in the DOS, with its lower edge lying 4 meV above the Fermi level. Notation: Γ, X, Y, and Z have their conventional meanings. S = $(\pi/a,\pi/b,0)$, U = $(\pi/a,0,\pi/c)$, R = $(\pi/a,\pi/b,\pi/c)$, and T = $(0,\pi/b,\pi/c)$.

these functionals do overestimate the ordered moment in TiAu, GGA by considerably more than LDA. For this reason, we try to account for this overestimate by applying the procedure suggested by Ortenzi *et al.* [19], as discussed in Sec. V.

III. ANALYSIS OF RESULTS

A. Band dispersion and density of states

The nonmagnetic band structure and atom-projected density of states (pDOS) and total DOS $N(E)$ of TiAu are displayed in Fig. 2. The DOS was presented earlier by Svanidze *et al.* [9] and is consistent with our result (which we have converged more highly due to the extremely fine structure). The bands along symmetry lines seem conventional for a metal, with several Fermi level (E_F) crossings. Near degeneracy of four bands very near E_F at R is uncommon but has no apparent impact. The bands below and at E_F have low (0.1–0.3 eV) dispersion along Γ-Z, reflecting some degree of quasi-two-dimensionality in the $\vec{a}$-$\vec{b}$ plane. However, there is enough dispersion across E_F that the Fermi surfaces (FSs) are three dimensional.

The DOS is prosaic for the most part, with expected features being present. The Au 5d bands are completely filled, centered 5 eV below E_F and 3 eV wide, so they are inert for magnetic and low-energy behavior. It might therefore be concluded that Au simply provides only its single s electron to the itinerant bands much as an alkali atom would do. We checked this simple picture by replacing Au with K, keeping the structure fixed. The Ti 3d bands (see below) remain at the same filling but the dispersion and FSs are substantially different. Therefore Au does play a specific role in determining the properties of TiAu.

The Fermi level lies within the 3-eV-wide Ti 3d bands, which are separated from the Au 5d bands by a pseudogap centered 2.5 eV below the Fermi level. The pseudogap region −3 to −1.5 eV contains roughly 0.3 electrons/f.u. At the broadest level, Au provides an itinerant electron gas, within which Ti with its open 3d shell resides.

The one remarkable aspect of this electronic structure is an extremely sharp and narrow DOS peak that is centered a few meV above the Fermi energy. Such a narrow peak requires two vHs lying nearby in energy, very similar to what occurs in the new highest temperature superconductor H_3S [20]. There are in fact several vHs within 35 meV of E_F, as discussed in the next subsection. The Fermi level DOS is $N(E_F) =$ 2.41 states/eV per spin and per f.u. (These units will be used for $N(E)$ throughout, for reasons to be explained in Sec. IV.B.) Thus the total DOS for both spins is 9.8 states/eV. This large value of $N(E_F)$ is very similar to the per-Ti value in $TiBe_2$, which also has a strong and narrow peak [21] in $N(E)$ at E_F and is also shows weak magnetic order. Various types of electronic-driven instabilities are suggested by such peaks.

Possible broken symmetries include (i) a Peierls instability, in which a lattice distortion splits the DOS peak and stabilizes the system by lowering $N(E_F)$, (ii) a superconducting instability, which is strongly encouraged by large $N(E_F)$ and gaps the Fermi surface in the superconducting state, (iii) a ferromagnetic instability, which provides an exchange splitting of majority and minority states and moves the DOS peak in each spin channel away from the Fermi level, and (iv) an excitonic state involving pairing across two or more vHs. Instabilities such as charge or orbital order might also be considered. Experimental data indicate [9] that it is the magnetic instability that wins this competition to stabilize the system by splitting the DOS peak away from E_F. It is, however, an AFM phase rather than the FM state that is observed. The underlying mechanism, critical scattering at very low energy and for the wave vector spanning the participating vHs, has been proposed and supported elsewhere [15].

B. van Hove singularities

The DOS peak results from two nearby vHs: vHs_1 at 4 meV and vHs_2 at 6 meV, relative to E_F. There are four more nearby vHs, at 15, 22, 28, and 34 meV. Most of these are evident in the inset of Fig. 2, where $N(E)$ is shown in the region near E_F. All lie where Ti 3d orbitals dominate, and the orbital characters of the vHs are a similar admixture. vHs_1, nearest to E_F and most responsible for the large value of $N(E_F)$, is discussed in detail

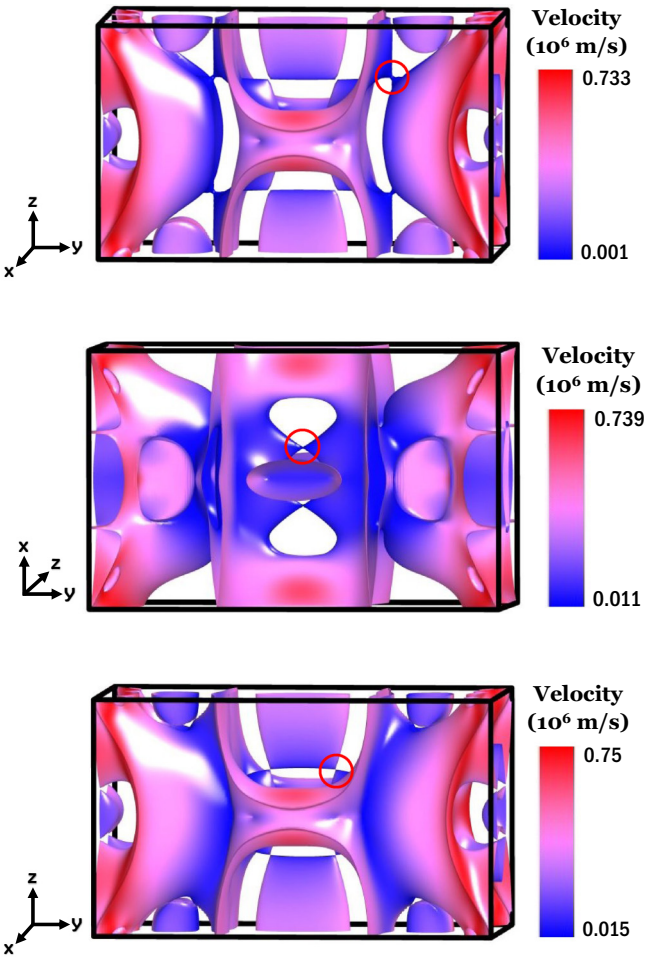

FIG. 3. The constant energy surfaces at the three M_1 or M_2 vHs discussed in the text. The energies relative to E_F are top, 4 meV; middle, 15 meV; and bottom, 34 meV. The coordinate system has been rotated in the middle panel so the double-cone surfaces can be seen, and the Γ point lies in the center of each figure. The velocities range from zero to $\sim 7.5 \times 10^7$ cm/s, with large (blue) sections having very low velocities, finally extending to zero at the singularities.

below, since it has been proposed that scattering between these mirrored vHs drive the AFM ordering [15]. The vHs at 15 meV lies at $(\pm 0.22\pi/a, 0, 0)$, giving only a pair of symmetry-related points. At 32 meV, the vHs lies in a symmetry plane giving four points $(0, \pm 0.16\pi/b, \pm 0.36\pi/c)$. The corresponding constant energy surfaces are pictured in Fig. 3. These surfaces, like the Fermi surface which is much like that for vHs_1, are large and multisheeted, with substantial areas of the largest sheets comprised of states with small velocity, less than 10^7 cm/s and extending to vanishingly small values at the vHs singularities. The maximum velocity on these sheets is 7.5×10^7 cm/s.

The vHs_1 point nearest E_F is of the M_1 type with two positive and one negative masses, with energy dispersion relative to the vHs

$$\varepsilon_k = \frac{k_x^2}{2m_x} - \frac{k_y^2}{2m_y} + \frac{k_z^2}{2m_z}. \quad (2)$$

M_1 and M_2 vHs display two-touching-cone constant energy surfaces at the vHs energies. These diabolical points, so named by Berry [22] in a somewhat different context, are visible in the constant energy surface plots pictured in Fig. 3. The position of this vHs_1 is $\vec{k}_0 = (0, 0.45\frac{\pi}{b}, 0.49\frac{\pi}{c})$ and symmetry-related points, being consistent with the Fermi level crossings in Fig. 2 that occur near $(0, \frac{b^*}{2}, 0)$ and $(0, 0, \frac{c^*}{2})$. The narrow band along Y-Γ-Z in Fig. 2 provides part of the low velocity surfaces but does not in itself give any hint of such a sharp and narrow peak in $N(E)$.

Due to the eight symmetry operations of space group $Pmma$, there are four vHs in the Brillouin zone, various of which are connected by the spanning vectors $\vec{Q}_{vHs} = (0, \pm 0.9\frac{\pi}{b}, \pm 0.98\frac{\pi}{c})$. The effective masses at vHs_1 are surprisingly heavy for an intermetallic Ti-Au compound of this type, $m_x = 21m_e$, $m_y = -4.5m_e$, $m_z = 4.9m_e$, and thus are consistent with a high DOS peak. The value of $N(E_{vHs})$ and thermodynamic properties are related to the thermal mass $m_{th} \equiv |m_x m_y m_z|^{1/3} = 7.7\, m_e$, a remarkably large value for an itinerant, presumably weakly correlated, intermetallic compound. The peak height arises from the heavy masses and the fact that the band remains relatively flat in the vHs region, providing a large phase space at that energy. Scattering between these regions are responsible for the maxima [15] in the nesting function $\xi_{\vec{q}}$, though the maxima are not nearly as impressive as FS nesting can produce, sometimes leading to a superconducting instability [23].

C. Magnetic instability

We have studied both FM and AFM phases, the latter with AFM wave vector $\vec{Q}_{AFM} = (0, \frac{\pi}{b}, 0)$. The FM moment on Ti is calculated to be $0.84\,\mu_B$ within GGA, consistent with previous findings [9]. Within LDA, the moment is $0.39\mu_B$, reflecting the delicacy of the moment in TiAu to the exchange correlation functional. As mentioned in Sec. II, a known feature of GGA versus LDA is to enhance and often overestimate magnetic tendencies. For this reason, we focus on the LDA results, from which we also consider further downward renormalization of the ordered moment in Sec. V.

We find (using LDA) that AFM alignment at $\vec{Q}_{AFM}$ is energetically favored over FM alignment by 3 meV, and over the nonmagnetic state by 11 meV, per Ti atom. The AFM moment is calculated to be $0.40\,\mu_B$/Ti within the Ti sphere similar to that for FM alignment, and not really consistent with an $S = \frac{1}{2}$ moment even considering reduction by the environment. Magnetism in TiAu is better pictured as itinerant rather than localized. The experimental value of the ordered moment is, however, only $0.15\,\mu_B$/Ti, a factor of almost three smaller. As mentioned earlier, for other weak magnets DFT predictions using a semilocal exchange functional have overestimated the magnetic moment. We return to these questions in Sec. V.

IV. VCA AND FSM CALCULATIONS

A. Virtual crystal approximation

Near QCPs, little understood processes arise that impact properties in peculiar ways [13]. We consider in this section changes with doping level x, confined to the mean field level.

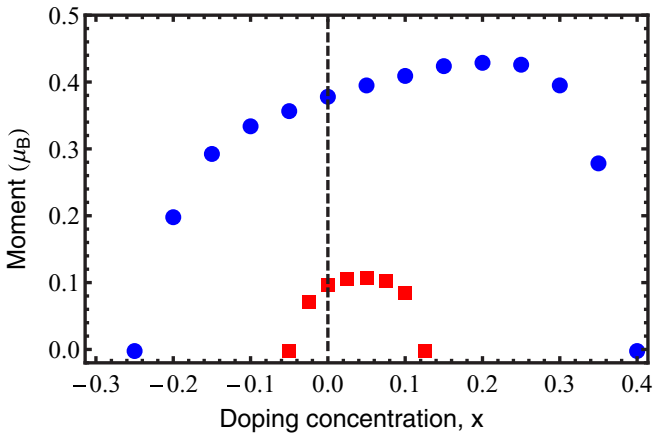

FIG. 4. Ferromagnetic tendency versus doping (x) by holes (Sc) and electrons (V), from the energy difference $\Delta E(x) = E_{nm} - E_{FM}$ between nonmagnetic and FM states. Blue dots (from LDA) do not account for spin fluctuations, while red dots take spin fluctuations into account by the Ortenzi procedure (see text). The peak corresponds to the peak in the density of states.

We apply the virtual crystal approximation (VCA) for the alloy electronic structure. In this treatment, for hole doping an average Ti-Sc nucleus with charge $22 - x$ is considered, and for electron doping an average Ti-V nucleus with charge $22 + x$ is chosen. Disorder is neglected but its effects are often small for doping with neighboring elements in intermetallic alloys, because the quantum behavior of electrons tends also to average over small local differences. Importantly, in VCA self-consistency of the addition (or depletion) of charge is taken into account, unlike the simpler rigid band approximation in which the Fermi level is simply moved to simulate the alloy's band structure.

The variation of ferromagnetic moment versus doping is summarized by the round (blue) symbols in Fig. 4. The moment decreases with hole doping, disappearing at a hole doping near 0.25. For electron doping, the LDA ordered moment increases initially as $E_F(x)$ moves across the vHs peak in $N(E)$ at $x = 0.06$. Surprisingly, it continues to increase beyond the DOS peak to $x = 0.25$, whereupon it dives rapidly to zero near $x = 0.40$.

Some asymmetry around E_F is expected because the Fermi level is situated somewhat below the peak in $N(E)$. The states in and around both vHs giving the peak are Ti d states, and the DOS is not so far from symmetric around the midpoint of the $N(E)$ peak to a distance of a few tenths of eV. However, the moment versus chemical potential is asymmetric. The other noteworthy aspect is the rapid drop of moment at each end (especially the electron doping end), seemingly approximating a first-order phase boundary versus the expected second-order (continuous) behavior in a mean field treatment. In these regions, achieving self-consistency becomes increasingly problematic, so we have not attempted to resolve the first- versus second-order issue. For $x = 0.35$, for example, the Fermi level lies at a sharp peak for one spin direction and a valley for the other spin direction; such a situation may complicate self-consistency. Also, the sharp drop in $N(E)$ on either side of the peak may be responsible.

The predictions from VCA then are that the doping concentrations corresponding to the quantum critical points, supposing FM order, are given in Fig. 4: 25% for hole doping and 40% for electron doping. The electronic structure and therefore the critical doping concentrations may be different for AFM order. The effect of spin fluctuations on these critical concentrations is the topic of Sec. V.

B. Fixed spin moment study

The DFT-based theory of the spin susceptibility [24] and of the ferromagnetic instability [25–27] formalizes the Stoner model, where an interelectron exchange interaction $\mathcal{I}$ encourages FM splitting of bands resisted by the increase in band ("kinetic") energy entailed by the splitting. The DFT prescription [24] for $\mathcal{I}$ was studied by Janak [25] and calculated for elemental transition metals.

Fixed spin moment calculations (FSM), wherein the electronic system is relaxed within DFT subject to the constraint of a chosen moment M, not only provides confirmation of the FM tendencies but conventionally enables identification of the DFT spin interaction (Stoner) constant $I(\vec{q} = 0) = \mathcal{I}$ for the functional being used. See the appendix for the definition of $I(\vec{q})$. FSM calculations were carried out to obtain the energy as a function of magnetic moment

$$E(M) = E(0) + \tfrac{1}{2}\chi^{-1}M^2 + \tfrac{1}{4}\beta M^4 + \cdots . \tag{3}$$

From the relation $d^2E/dM^2 = \chi^{-1}$ the Stoner enhancement of susceptibility S due to the exchange interaction is conventionally obtained according to

$$\chi = \frac{\chi_0}{1 - \mathcal{I}N(E_F)} \equiv S\chi_0, \tag{4}$$

where the bare susceptibility per f.u. is $\chi_0 = 2\mu_B^2 N(E_F)$ in terms of the unpolarized $N(E)$. We note that $N(E)$ always refers to the DOS per spin and per f.u. (i.e., per Ti atom). In this form, $\mathcal{I}$ has the interpretation as the Ti atomic value. Various conventions have been used in the literature. Vosko and Perdew [24] and Janak [25] used the DOS for both spins multiplying $\mathcal{I}$ in Eq. (4), so their values of $\mathcal{I}$ must be doubled when comparing with values for the convention used here, which were also used by Andersen *et al.* [27] and Krasko [28].

The LDA FSM results are shown in Fig. 5. For undoped TiAu, the LDA value of magnetic moment at the minimum of energy is equal to the moment from the FM calculation ($M = 0.39\mu_B$), as it must be. However, for such strong structure in $N(E)$ near E_F the small M limit of various quantities, including the expansions of $E(M)$, requires calculating and fitting at very small values of M, less than $0.02\mu_B$, as we show below. Such calculations are challenging and, as we argue below, unnecessary. Another consequence of the vHs-induced energy variation is that the constant (or slowly varying) $N(E)$ expression [26] for the Ti moment $M = N(E_F)\Delta_{\rm ex}$ is replaced by $M = \bar{N}(M)\Delta_{\rm ex}$, where $\Delta_{\rm ex} = E_{F,\uparrow} - E_{F,\downarrow}$ is the band exchange splitting and $\bar{N}(M)$ is the average DOS over this range of splitting. Note that the Fermi energies for up and down spins, $E_{F,\uparrow}$ and $E_{F,\downarrow}$, are no longer equally displaced from the $M = 0$ Fermi level.

In Fig. 6, this average DOS $\bar{N}(M)$ is displayed, showing a peak rise by 2% at $M = 0.03\mu_B$ due to the DOS peak above

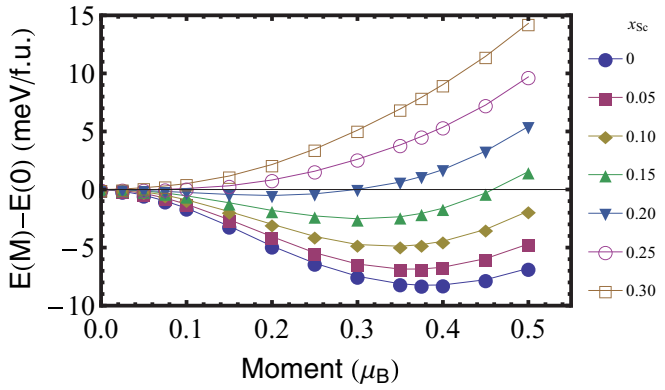

FIG. 5. Fixed spin moment energy of TiAu as a function of moment M at various hole dopings x (legend is at the right), using the LDA functional.

E_F, followed by a precipitous drop to half its original value for $M = 0.6\mu_B$ and larger. Since the slope of $E[M]$ must be negative [27,28] as well as the Stoner criterion (above) being satisfied, to promote a FM instability, this curve indicates an instability for any value of $\mathcal{I}$ in the range $0.4\,\text{eV} \leqslant \mathcal{I} \leqslant 0.8\,\text{eV}$, corresponding to (imposed) moments of $0.03 \leqslant M \leqslant 0.9$. The energy minimum determines the most favored moment.

As mentioned, the curvature obtained from the customary FSM plot for TiAu, the $x = 0$ curve on the scale of Fig. 5, does not allow a reliable estimate of χ^{-1} and hence the Stoner enhancement in the small M limit, and thus not of $\mathcal{I}$ itself, without a challenging calculation for tiny moments. However, $\mathcal{I}$ is determined by derivatives of the exchange-correlation functional and wave function character at the Fermi level [25] and should be slowly varying within energy regions dominated by Ti $3d$ character, as is the case we are exploring.

As the hole doping x increases the corresponding Fermi level moves away from the DOS peak, making the fine structure progressively less relevant. We calculate the FM instability to disappear at $x = x_{cr} = 0.25$, where the Fermi level is 73 meV lower than for TiAu ($x = 0$), well away from the vHs. At

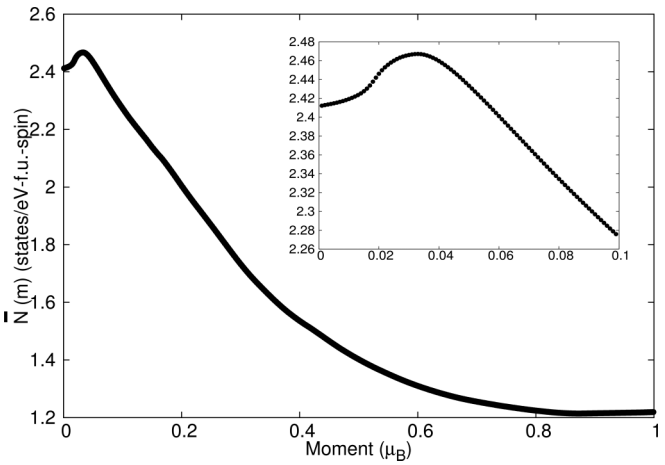

FIG. 6. The density of states $\bar{N}(M)$ averaged over the range $E_{F,\downarrow}$ to $E_{F,\uparrow}$ contributing to moment M, versus Ti moment M. The inset shows the fine structure at small M arising from the vHs.

this Stoner critical point, $\mathcal{I} = 1/N(E_F,x_{cr})$ without any need for curve fitting. Here $N(E_F,x_{cr}) = 1.35$ states/(eV spin f.u.) gives $\mathcal{I} = 0.74\,\text{eV}$, similar to Janak's value for elemental Ti after accounting for his factor of two convention. This value then gives the Stoner product for TiAu of $\mathcal{I}N(E_F,x = 0) = 1.8$, reflecting a very strong FM instability. Nonetheless, experiment shows that AFM alignment wins the competition for the ground state, as also confirmed by our LDA calculations.

V. ACCOUNTING FOR SPIN FLUCTUATIONS

The overestimation of magnetic moment by DFT functionals is understood from the viewpoint that they do not take account of the type of spin fluctuations that must be occurring in weak magnets such as TiAu. Effects of spin fluctuations can be modeled from a Landau viewpoint, leading to a suppression of ordering tendency and of the ordered moment in DFT.

Moriya's self-consistent renormalization (SCR) theory [10,11] of spin fluctuations provides the modern theory of weak magnetism due largely to the fact that (i) the C-W behavior of $\chi(q = 0)$ is not explained by Stoner theory and (ii) RPA theory requires modification at higher temperatures. Moriya's SCR theory not only resolved these difficulties, but it also predicted some observed quantum critical behavior of wFMs as well, for example, $1/\chi_Q \to T^{3/2}$ and $C_m/T \to \propto T^{1/2}$ for a 3D AFM system [14]. In a wAFM system, since the most important effect of the spin fluctuations comes from the small q (relative to the ordering $\vec{Q}$ vector) and small ω region, the dynamical susceptibility $\chi(\vec{Q} + \vec{q},\omega)$ is expanded as described in the appendix. The coefficients depend on the particular band structure, and unfortunately Moriya's theory [29] is only semiquantitative as it depends on ill-defined cutoffs.

Ortenzi *et al.* suggested [19] that a simple magnetic renormalization procedure can account for the fluctuations, appearing as a scaling factor s, $0 < s < 1$, of the spin-dependent part of the exchange correlation functional. The scaling factor s is not easy to determine from first principles, but it can be fixed by tuning it to reproduce the experimental moment. This method is implemented in the WIEN2K code [30]. We find that with a scale factor $s = 0.55$, the LDA magnetic moment is reduced to the experimental value of $0.15\mu_B$/Ti. The corresponding AFM electronic structure can be found in Ref. [15].

With the Ortenzi spin fluctuation scaling, the magnetic tendency is comparably reduced. Figure 4 provides a comparison of the FM moment when alloying within this exchange scaled theory within LDA. For $s = 0.55$, magnetism disappears at a hole doping of 0.05 and an electron doping of 0.13, smaller by factors of five and three, respectively, than the LDA results. It will be revealing to learn how accurate these predictions for FM TiAu compare with the critical doping levels for the observed AFM phase, if alloying to the critical points can be achieved.

VI. DISCUSSION AND SUMMARY

The electronic structure and magnetic tendencies of the weak antiferromagnet TiAu have been studied using *ab initio* methods. The dominant feature of the paramagnetic phase is a very sharp and narrow peak in the DOS at the Fermi level, arising from a van Hove singularity involving unexpectedly large masses for an intermetallic Ti-Au compound. This

peak provides a strong Stoner instability to ferromagnetism, yet the observed magnetic order is simple commensurate antiferromagnetic order, $\vec{Q}_{AFM} = (0, \frac{\pi}{b}, 0)$, a result that is upheld by DFT calculations.

Both FM and AFM magnetically ordered states were obtained and studied, with the AFM state lying lower in energy consistent with observation. Within LDA the ordered magnetic moment is calculated to be 2.7 times larger than found in neutron diffraction, so the phenomenological spin fluctuation reduction of Ortenzi *et al.* was applied. Why is AFM order favored over FM? Our previous work [15] provided evidence that mirrored vHs provides enhanced low-q, small-ω fluctuations that make AFM more favorable than otherwise and that the AFM phase is further stabilized by the exchange splitting of flat bands above and below the Fermi level along two symmetry lines in the AFM Brillouin zone.

The response of the nonmagnetic system to both hole and electron doping was studied within the virtual crystal approximation for the FM phase, using both LDA and the Ortenzi renormalization. Analysis of the VCA results allows identification of the Stoner exchange constant $\mathcal{I} = 0.74$ eV. Fixed spin moment studies were provided to provide a better understanding of the interplay between the van Hove peak and the Stoner instability. The Ortenzi rescaling by 45% to account phenomenologically for spin fluctuations reduces the predicted FM quantum critical points (critical doping concentrations in Fig. 4) severely, by a factor of three to five. The critical dopings for the observed AFM order may differ, so experimental doping studies will be of interest. This system could provide an important platform for further exploration of AFM quantum critical points.

ACKNOWLEDGMENTS

We acknowledge helpful conversations with Y. Quan, K.-W. Lee, A. S. Botana, and S. Gangopadhyay, and comments on weak magnetism from V. Taufour. Our research used resources of the National Energy Research Scientific Computing Center (NERSC), a DOE Office of Science User Facility supported by the Office of Science of the US Department of Energy under Contract No. DE-AC02-05CH11231. This work was supported by National Science Foundation consecutive Grants No. DMR-1207622 and No. DMR-1607139.

APPENDIX

Here we review some of the formalism underlying spin fluctuation theory that is Fermi surface related. As we quantify below, nonmagnetic TiAu has a very strong ferromagnetic (FM) instability at $q = 0$ and a few possible nesting wave vectors for spin density wave order [9], yet the observed magnetic order is simple AFM with wave vector $\vec{Q}_{AFM} = \vec{b}^*/2$ at a zone boundary. The likelihood of competing instabilities leads us to review some of the formalism of the treatment of spin fluctuations in the neighborhood of the transition temperature, for low frequencies ω and for wavelengths near the ordering wave vector.

The quantity of interest is the magnetic susceptibility χ, with the objective of connecting to material-specific information from density functional theory (DFT). Following the formulation of Janak [25] for the interacting static, macroscopic susceptibility within DFT and the extension by Gross *et al.* [31] to the dynamic, microscopic counterpart $\chi(q,\omega)$, the expression appearing in random phase approximation form but valid more generally is

$$\begin{aligned}\chi(q,\omega) &= \frac{\chi_o(q,\omega)}{1 - I(q)\chi_o(q,\omega)},\\ I(q) &= \frac{1}{2}\mathcal{F}\left\langle \frac{\delta^2 E_{xc}[n,m]}{\delta m(r)\delta m(r')}\right\rangle_q\\ \chi^{-1}(q,\omega) &= \chi_o^{-1}(q,\omega) - I(q),\end{aligned} \tag{A1}$$

where $\mathcal{F}$ indicates the Fourier transform. The vector notation on vectors will be dropped here for simplicity except when needed for emphasis, and we take $\hbar = 1$. The $q = 0$ expression can be found in Janak's paper [25]. A formally exact expression is similar, but requires quantities to be matrix elements in reciprocal lattice vectors and a frequency-ω-dependent exchange-correlation interaction $I(q,\omega)$. For the small ω of interest in this paper, the frequency dependence of $I(q,\omega)$ can be omitted. Here $E_{xc}[n,m]$ is the exchange-correlation energy function of charge density $n(r)$ and magnetization density $m(r)$, and χ_o is the noninteracting Kohn-Sham (viz. Lindhard form) susceptibility.

The Kohn-Sham susceptibility is ($\hbar = 1$)

$$\chi_o(q,\omega) = \sum_{k,m,n} |M_{k,m;k+q,n}|^2 \frac{f_{k,n} - f_{k+q,m}}{\varepsilon_{k,n} - \varepsilon_{k+q,m} - \omega - i\eta}, \tag{A2}$$

in terms of the Kohn-Sham eigenvalues ε_{kn}, and η is a positive infinitesimal. $M_{k,m;k+q,n}$ is the matrix element of $\exp(iq\cdot r)$ between Bloch states. For crystals the susceptibilities become matrices in reciprocal lattice vectors and the resulting local field effects can be important for quantitative detail, but our treatment will not extend to that level.

1. FM case

The small q,ω expansion (for orthorhombic symmetry) is

$$\chi_o(q,\omega) = \chi_o + \sum_j A_j q_j^2 + i\left\langle \frac{1}{\hat{q}\cdot v}\right\rangle_{FS}\frac{\omega}{q}, \tag{A3}$$

the last expression being appropriate for $\omega < v_F q$. The expressions for the coefficients have been presented in the literature [10,21]

$$\begin{aligned}A_j &= -\frac{1}{12}\frac{d}{d\varepsilon}\left[N(\varepsilon)\left\langle\frac{\partial v_{k,j}}{\partial k_j}\right\rangle\right]\\ &= \frac{1}{48\pi e^2}\left(\frac{2\pi}{a_j}\right)^2\frac{d^2\Omega^2_{p,j}(E_F)}{dE_F^2},\end{aligned} \tag{A4}$$

where $\vec{v}_k = \nabla_k \varepsilon_k$ is the band velocity. The second expression for A_j incorporates the Drude plasma energy

$$\Omega^2_{p,j}(E_F) = 4\pi e^2 N(E_F) v_j^2(E_F) \tag{A5}$$

in terms of the mean square Fermi surface velocity $v_j^2(E_F)$.

The first expression for A_j is instructive when E_F is near the van Hove singularity E_{vHs}. In that case the second derivatives are just the vHs effective masses, and for the positioning of

E_F in TiAu (see Sec. IV), $N(\varepsilon) \propto -m_{th}^{3/2}(E_{vHs} - \varepsilon)^{1/2}$. Then the contribution from the vHs region is

$$A_j^{vHs} \propto -\frac{1}{24}\frac{m_{th}^{3/2}}{m_j}\frac{1}{\sqrt{E_{vHs} - E_F}}, \tag{A6}$$

which becomes divergent at the vHs.

2. AFM case, $\vec{Q} > 0$

With spatial fluctuations at $q + Q$ around nonzero Q not being long wavelength, the expressions for the low-energy, small q coefficients are not all tied to the Fermi surface, so they are not as intuitive as for the FM $Q = 0$ case. At $\omega = 0$, the susceptibility is real and given for small q by (for ease in interpretation, the matrix elements are omitted)

$$\chi_o(Q + q, \omega = 0) = \chi_o(Q) + \sum_k \left[\frac{\delta(\varepsilon_{k+Q})}{\varepsilon_{kn} - \varepsilon_{k+Q,m}} + \frac{f_{kn} - f_{k+Q,m}}{(\varepsilon_{kn} - \varepsilon_{k+Q,m})^2}\right]\vec{v}_k \cdot \vec{q}. \tag{A7}$$

The first term is due to the change in band occupation with q, being a sum over over the FS of the inverse of occupied eigenvalues $\vec{Q}$ away from the FS, and is likely to vary slowly with Q unless it is small. The second term arises from the change with q in the energy denominator. Since it involves the energy difference squared, it is more likely to have strong Q dependence when $\vec{Q}$ is near a nesting wave vector. Expressions for the second-order terms in q^2,$q\omega$, and ω^2 are involved and unenlightening.

For small ω, the imaginary part becomes

$$\chi_o''(Q + q, \omega) = \pi\omega\xi(Q) - \pi\sum_k \delta(\varepsilon_k)\delta(\varepsilon_{k+Q})v_{k+Q} \cdot q$$
$$\xi(Q) = \sum_k \delta(\varepsilon_k)\delta(\varepsilon_{k+Q}). \tag{A8}$$

$\xi(Q)$ is the FS nesting function that measures the phase space available for scattering from the FS at k to the FS at $k + Q$, most often discussed in phonon scattering processes. Evidently small ω processes are focused into regions of nesting. $\xi(q)$ is evaluated and discussed in Ref. [15].

[1] P. Dalmas de Réotier, G. Lapertot, A. Yaouanc, P. C. M. Gubbens, S. Sakarya, and A. Amato, Evidence for an antiferromagnetic component in the magnetic structure of $ZrZn_2$, Phys. Lett. A **349**, 513 (2006).

[2] B. T. Matthias, A. L. Giorgi, V. O. Struebing, and J. L. Smith, Itinerant antiferromagnetism of $TiBe_2$, Phys. Lett. A **69**, 221 (1978).

[3] C. P. Enz, On the possibility of weak itinerant antiferromagnetism in $TiBe_2$, Physica B+C (Amsterdam, Neth.) **107**, 77 (1981).

[4] E. C. Stoner, Collective electron ferromagnetism, Proc. R. Soc. London, Ser. A **165**, 372 (1938).

[5] N. Gayathri, A. K. Raychaudhuri, S. K. Tiwary, R. Gundakaram, A. Arulraj, and C. N. R. Rao, Electrical transport, magnetism, and magnetoresistance in ferromagnetic oxides with mixed exchange interactions: A study of the $La_{0.7}Ca_{0.3}Mn_{1-x}Co_xO_3$ system, Phys. Rev. B **56**, 1345 (1997).

[6] S. Raymond, J. Floquet, R. Calemczuk, L. P. Regnault, B. Fak, P. Haen, S. Kambe, P. Lejay, and T. Fukuhara, Neutron scattering of fragile antiferromagnetic phases in heavy fermion compounds, Physica B (Amsterdam, Neth.) **280**, 354 (2000).

[7] B. G. Ueland, A. Kreyssig, K. Prokeš, J. W. Lynn, L. W. Harriger, D. K. Pratt, D. K. Singh, T. W. Heitmann, S. Sauerbrei, S. M. Saunders, E. D. Mun, S. L. Bud'ko, R. J. McQueeney, P. C. Canfield, and A. I. Goldman, Fragile antiferromagnetism in the heavy-fermion compound YbBiPt, Phys. Rev. B **89**, 180403(R) (2014).

[8] P. C. Canfield and S. L. Bud'ko, Preserved entropy and fragile magnetism, Rep. Prog. Phys. **79**, 084506 (2016).

[9] E. Svanidze, J. K. Wang, T. Besara, L. Liu, Q. Huang, T. Siegrist, B. Frandsen, J. W. Lynn, A. H. Nevidomskyy, M. B. Gamza, M. C. Aronson, Y. J. Uemura, and E. Morosan, An itinerant antiferromagnetic metal without magnetic constituents, Nat. Commun. **6**, 7701 (2015).

[10] T. Moriya and Y. Takahashi, Spin fluctuations in itinerant electron magnetism, J. Phys. Colloq. **39**, 1466 (1979).

[11] T. Moriya, *Spin Fluctuations in Itinerant Electron Magnetism* (Springer, Berlin, 1985).

[12] R. Konno, The self-consistent renormalization theory of longitudinal spin fluctuations for weak antiferromagnetic metals with degenerate bands, Czech. J. Phys. **46** (Suppl. S4), 1842 (1996).

[13] H. V. Löhneysen, A. Rosch, M. Vojta, and P. Wölfle, Fermi-liquid instabilities at magnetic quantum phase transitions, Rev. Mod. Phys. **79**, 1015 (2007).

[14] T. Moriya and K. Ueda, Antiferromagnetic spin fluctuation and superconductivity, Rep. Prog. Phys. **66**, 1299 (2003).

[15] W. F. Goh and W. E. Pickett, A mechanism for weak itinerant antiferromagnetism: Mirrored van Hove singularities, Europhys. Lett. **116**, 27004 (2016).

[16] K. Koepernik and H. Eschrig, Full-potential nonorthogonal local-orbital minimum-basis band-structure scheme, Phys. Rev. B **59**, 1743 (1999).

[17] J. P. Perdew and Y. Wang, Accurate and simple analytic representation of the electron-gas correlation energy, Phys. Rev. B **45**, 13244 (1992).

[18] J. P. Perdew, K. Burke, and M. Ernzerhof, Generalized Gradient Approximation Made Simple, Phys. Rev. Lett. **77**, 3865 (1996).

[19] L. Ortenzi, I. I. Mazin, P. Blaha, and L. Boeri, Accounting for spin fluctuations beyond local spin density approximation in the density functional theory, Phys. Rev. B **86**, 064437 (2012).

[20] Y. Quan and W. E. Pickett, Van Hove singularities and spectral smearing in high temperature superconducting H_3S, Phys. Rev. B **93**, 104526 (2016).

[21] T. Jeong, A. Kyker, and W. E. Pickett, Fermi velocity spectrum and incipient magnetism in $TiBe_2$, Phys. Rev. B **73**, 115106 (2006).

[22] M. V. Berry, Aspects of degeneracy, in *Chaotic Behavior in Quantum Systems*, edited by G. Casatil (Plenum, New York, 1985), pp. 123–140.

[23] D. Kasinathan, J. Kuneŝ, A. Lazicki, H. Rosner, C. S. Yoo, R. T. Scalettar, and W. E. Pickett, Superconductivity and Lattice

Instability in Compressed Lithium from Fermi Surface Hot Spots, Phys. Rev. Lett. **96**, 047004 (2006).

[24] S. H. Vosko and J. P. Perdew, Theory of the spin susceptibility of an inhomogeneous electron gas via the density functional formalism, Can. J. Phys. **53**, 1385 (1975).

[25] J. F. Janak, Uniform susceptibilities of metallic elements, Phys. Rev. B **16**, 255 (1977).

[26] O. Gunnarsson, Band model for magnetism of transition metals in the spin-density-functional formalism, J. Phys. F **6**, 587 (1976).

[27] O. K. Andersen, J. Madsen, U. K. Poulsen, O. Jepsen, and J. Kollar, Magnetic ground state properties of transition metals, Physica B (Amsterdam, Neth.) **86-88**, 249 (1977).

[28] G. I. Krasko, Metamagnetic behavior of fcc iron, Phys. Rev. B **36**, 8565 (1987).

[29] H. Hasegawa and T. Moriya, Effect of spin fluctuations on itinerant electron antiferromagnetism, J. Phys. Soc. Jpn. **36**, 1542 (1974).

[30] P. Blaha, K. Schwarz, G. K. H. Madsen, D. Kvasnicka, and J. Luitz, *WIEN2K: An Augmented Plane Wave + Local Orbitals Program for Calculating Crystal Properties* (Techn. Universität Wien, Austria, 2001).

[31] E. K. U. Gross and W. Kohn, Local Density-Functional Theory of Frequency-Dependent Linear Response, Phys. Rev. Lett. **55**, 2850 (1985).